# Spatio-Temporal Coding for Wireless Communication

Gregory G. Raleigh, *Member, IEEE*, and John M. Cioffi, *Fellow, IEEE*

***Abstract*—Multipath signal propagation has long been viewed as an impairment to reliable communication in wireless channels. This paper shows that the presence of multipath greatly improves achievable data rate if the appropriate communication structure is employed. A compact model is developed for the multiple-input multiple-output (MIMO) dispersive spatially selective wireless communication channel. The multivariate information capacity is analyzed. For high signal-to-noise ratio (SNR) conditions, the MIMO channel can exhibit a capacity slope in bits per decibel of power increase that is proportional to the minimum of the number multipath components, the number of input antennas, or the number of output antennas. This desirable result is contrasted with the lower capacity slope of the well-studied case with multiple antennas at only one side of the radio link. A spatio-temporal vector-coding (STVC) communication structure is suggested as a means for achieving MIMO channel capacity. The complexity of STVC motivates a more practical reduced-complexity discrete matrix multitone (DMMT) space–frequency coding approach. Both of these structures are shown to be asymptotically optimum. An adaptive-lattice trellis-coding technique is suggested as a method for coding across the space and frequency dimensions that exist in the DMMT channel. Experimental examples that support the theoretical results are presented.**

***Index Terms*—Adaptive arrays, adaptive coding, adaptive modulation, antenna arrays, broad-band communication, channel coding, digital modulation, information rates, MIMO systems, multipath channels.**

## I. Introduction

THE SYSTEMATIC study of reliable communication in linear channels was initiated by the work of Shannon in 1948 [1]. The information capacity of certain multiple-input multiple-output (MIMO) channels with memory was derived by Brandenburg and Wyner [2]. Recent work by Cheng and Verdu [3] derives the capacity region for more general multiaccess MIMO channels. The problem of joint optimization of a multivariate transmitter–receiver pair to minimize the mean-square error criteria (MMSE) has gained considerable attention. One of the earliest contributions to this problem was made by Salz [4], who developed the optimum linear MMSE vector transmission and reception filters for $M \times M$ channels with no excess bandwidth. More recent work on MIMO equalizers includes the linear equalizer with excess bandwidth and the decision feedback equalizer [5]–[7].

Consider the problem of communication with linear modulation in a frequency-dispersive spatially selective wireless channel $\boldsymbol{H}$ composed of $M_T$ transmission antennas and $M_R$ reception antennas with additive noise. What is the impact of multipath on the information capacity of the discrete time communication channel? How do various multiple antenna structures influence channel capacity? Is it possible to construct multiple antenna coding systems that benefit from the inherent properties of severe multipath channels? This paper is a first attempt to answer these questions for time-invariant channels such as those that exist in certain wireless local loop applications. Time-varying channels are treated in [8] and [9].

A compact MIMO channel model is developed in Section II. We then explore the theoretical information capacity limits of the MIMO channel in Section III. We find that multipath substantially improves capacity for the MIMO case. Specifically, if the number of multipath components exceeds a certain value, then the channel capacity slope in bits per decibel of power increase can be proportional to the number of antennas located at both the input and output of the channel. This highly desirable result is contrasted with the more conventional case with multiple antennas on only one side of the channel. A spatio-temporal vector coding (STVC) structure for burst transmission is suggested as a theoretical means for achieving capacity. The high complexity of the STVC structure motivates a more practical reduced-complexity discrete matrix multitone (DMMT) space–frequency coding structure which is analyzed in Section IV. Both STVC and DMMT are shown to achieve the true channel capacity as the burst duration increases. In Section V, an adaptive-lattice trellis-coding technique is suggested as a practical method for coding across space and frequency dimensions in the DMMT channel. Experimental examples that support the theoretical results are then reported in Section VI.

The main contributions in this paper are the matrix channel model development, the connection between rank and multipath shown in Lemma 1, the multipath capacity behavior of various multiple antenna structures highlighted by Corollaries 2 and 3, introduction of DMMT as a realizable means to achieve a multiplicative reliable rate advantage in dispersive MIMO channels, and the asymptotic optimality proof for DMMT capacity Theorem 2. The results presented in this paper are based on the work previously reported in [10]–[12].

Paper approved by T. Aulin, the Editor for Coding and Communication Theory of the IEEE Communications Society. Manuscript received April 9, 1996; revised September 27, 1996 and July 21, 1997. This work was supported by Watkins-Johnson Company and by Clarity Wireless, Inc. This paper was presented in part at the 1996 Global Communications Conference, November 1996.

G. G. Raleigh is with Clarity Wireless, Inc., Belmont, CA 94002 USA (e-mail: raleigh@clarity-wireless.com).

J. M. Cioffi is with the Department of Electrical Engineering, Stanford University, Stanford, CA 94305-4055 USA, and with Amati Communications Corporation, San Jose, CA 95124 USA.

Publisher Item Identifier S 0090-6778(98)02123-0.

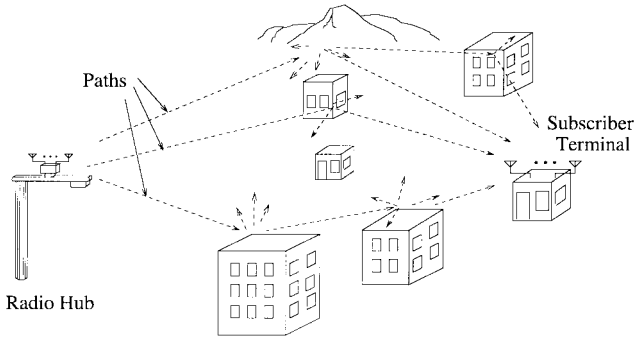


Fig. 1. Illustration of the physical wireless channel.

## II. MIMO Channel Model

Wireless communication channels are often characterized by severe multipath [13], [14]. The transmitted signal propagates along $L$ multiple paths created by reflection and scattering from physical objects in the terrain as illustrated in Fig. 1. We derive a far field[1] signal model for linearly modulated digital communication for a system with $M_T$ transmitting antennas and $M_R$ receiving antennas. In all that follows, complex valued baseband signal models are used. The implicit assumption is that a radio frequency carrier upconverts the baseband communication signal which is transmitted over the air and then coherently demodulated back to baseband at the receiver.

Considering the propagation geometry for the $l$th propagation path, the $j$th transmit antenna gain response[2] due to the angle of departure $\theta_{tl}$ is $a_{t,j}$ and the $i$th receive antenna gain response due to angle of arrival $\theta_{R,l}$ is $a_{R,i}(\theta_{R,l})$. The $l$th propagation path is further characterized by a complex path amplitude $\beta_l$ and a path propagation delay $\tau_l$. This propagation geometry is depicted in Fig. 2.

In the context of a digital signaling scheme, the transmitted baseband signal for the $j$th transmitter element is

$$s_j(t) = \sum_n z_j(n) g(t - nT)$$

where $\{z_j(n)\}$ is the (complex) symbol sequence, $g(t)$ is the pulse shaping function impulse response, and $T$ is the symbol period. The pulse shaping function is typically the convolution of two separate filters, one at the transmitter and one at the receiver. The optimum receiver filter is a matched filter. In practice, the pulse shape is windowed, resulting in a finite duration impulse response. The received signal for the $i$th antenna is then

$$x_i(t) = \sum_{j=1}^{M_T} \sum_{l=1}^{L} \beta_l a_{T,j}(\theta_{T,l}) a_{R,i}(\theta_{R,l}) \cdot \sum_n z_j(n) g(t - nT - \tau_l) + n_i(t)$$

where $n_i(t)$ is the additive receiver noise.

[1] Here, the far field assumption implies that dominant reflectors are sufficiently far from the arrays so that the angles of departure, angles of arrival, and time delays are constant over the extent of the array aperture.

[2] Azimuth plane path propagation angles are considered here. The models can easily be extended to include the effects of elevation angle by simply adding a second angular coordinate.

Synchronous complex baseband sampling with symbol period $T$ is assumed for the receiver. We define $n_0$ and $(\nu+1)$ to be the maximum lag and length over all $l$ for the sampled pulse function sequences $\{g(nT - \tau_l)\}$. To simplify notation, it is assumed that $n_0 = 0$, and the discrete-time notation $g(nT - \tau_l) = g_l(n)$ is adopted.

When a block of $N$ data symbols are transmitted, $N + \nu$ nonzero output samples result, beginning at time sample $k - N + 1$ and ending with sample $k + \nu$. The composite channel output can now be written as a column vector with all time samples for a given receive antenna appearing in order so that $\boldsymbol{x}(k) = [x_1(k-N+1) \cdots x_1(k+\nu) \cdots x_{M_R}(k-N+1) \cdots x_{M_R}(k+\nu)]^T$, with an identical stacking for the output noise samples $\boldsymbol{n}(k)$. The input symbol vector is written $\boldsymbol{z}(k) = [z_1(k-N+1) \cdots z_1(k) \cdots z_{M_T}(k-N+1) \cdots z_{M_T}(k)]^T$. The spatio-temporal channel may then be expressed as a vector equation

$$\boldsymbol{x}(k) = \boldsymbol{H}\boldsymbol{z}(k) + \boldsymbol{n}(k) \tag{1}$$

where the MIMO channel matrix is composed of $(N+\nu) \times N$ single-input single-output (SISO) subblocks

$$\boldsymbol{H} = \begin{bmatrix} \boldsymbol{H}_{1,1} & \cdots & \boldsymbol{H}_{1,M_T} \\ \vdots & \ddots & \vdots \\ \boldsymbol{H}_{M_R,1} & \cdots & \boldsymbol{H}_{M_R,M_T} \end{bmatrix} \in \mathbb{C}^{(N+\nu)\cdot M_R \times N \cdot M_T}$$

with each subblock possessing the well-known Toeplitz form. To clearly illustrate the effect of multipath, the channel can be written as the sum over multipath components[3]

$$\boldsymbol{H} = \sum_{l=1}^{L} \beta_l \begin{bmatrix} a_{R,1}(\theta_{R,l}) \boldsymbol{I}_{(N+\nu)} \\ \vdots \\ a_{R,M_R}(\theta_{R,l}) \boldsymbol{I}_{(N+\nu)} \end{bmatrix} \cdot \boldsymbol{G}_l [a_{T,1}(\theta_{T,l}) \boldsymbol{I}_N \cdots a_{T,M_T}(\theta_{T,l}) \boldsymbol{I}_N] \tag{2}$$

where the $(N+\nu) \times N$ Toeplitz pulse shaping matrix is

$$\boldsymbol{G}_l = \begin{bmatrix} g_l(0) & 0 & 0 & 0 & \cdots & 0 \\ \vdots & \ddots & \ddots & \ddots & \ddots & \vdots \\ g_l(\nu) & \cdots & g_l(0) & 0 & \cdots & 0 \\ 0 & g_l(\nu) & \cdots & g_l(0) & 0 & 0 \\ \vdots & \ddots & \ddots & \ddots & \ddots & \vdots \\ 0 & \cdots & 0 & g_l(\nu) & \cdots & g_l(0) \\ \vdots & \ddots & \ddots & \ddots & \ddots & \vdots \\ 0 & \cdots & 0 & 0 & 0 & g_l(\nu) \end{bmatrix}. \tag{3}$$

This channel description is illustrated in Fig. 3.

*Lemma 1:* The number of finite amplitude parallel spatio-temporal channel dimensions $K$ that can be created to communicate over the far field channel described by (1) is bounded by

$$K \le \min(N \cdot L, (N+\nu) \cdot M_R, N \cdot M_T). \tag{4}$$

[3] In (2), the inherent assumptions are that each propagation path amplitude $\beta_l$, and the transmit and receive antenna array responses $a_{T,j}(\theta_{T,l})$ and $a_{R,i}(\theta_{R,l})$, are frequency invariant over the fractional bandwidth of the signal. While these assumptions are not necessary, they simplify the discussion.

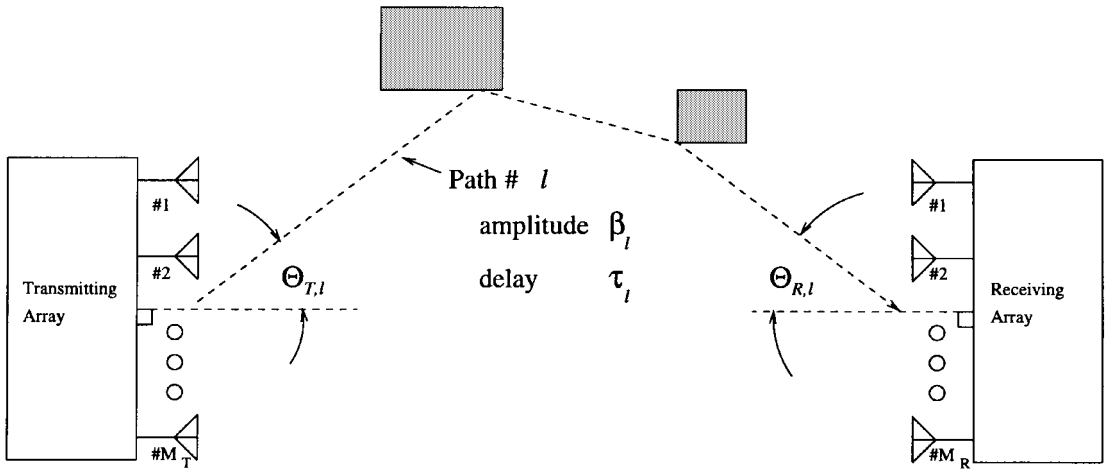


Fig. 2. Propagation path geometry.

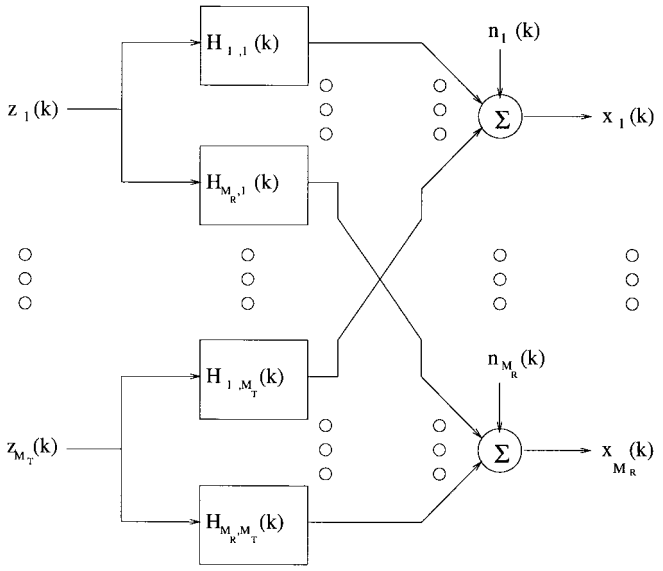


Fig. 3. Discrete-time MIMO channel diagram.

*Proof:* The channel matrix is expressed as the sum of $L$ component matrices in (2). By inspection, the left matrix in the expression has rank bounded by $N+\nu$, the middle matrix has rank $N$, and the right matrix has rank bounded by $N$. Each component matrix in the sum can then add at most rank $N$. For $NL < \min((N+\nu)M_R, NM_T)$, the rank of $\boldsymbol{H}$ is bounded by $NL$. For $NL > \min((N+\nu)M_R, NM_T)$, the composite matrix is bounded by the full rank condition of $\min((N+\nu)\cdot M_R, N\cdot M_T)$. ■

The two-dimensional spatio-temporal channel has been written as a compact one-dimensional vector expression with a block Toeplitz channel matrix. As we will see, this formulation will help make the difficult problem of communication in dispersive MIMO channels more tractable.

## III. Spatio-Temporal Channel Capacity

In this section we explore the information capacity for the spatio-temporal channel developed in the previous section. A theoretical STVC system is then suggested as a means for achieving capacity. We then derive the relationship between the MIMO channel capacity and the capacity of the underlying SISO, single-input multiple-output (SIMO), and multiple-input single-output (MISO) channels for the high signal-to-noise ratio (SNR)[4] case.

We proceed under three assumptions. The noise $\boldsymbol{n}(k)$ is additive white Gaussian (AWGN)[5] with covariance $\sigma^2\boldsymbol{I}_{M_R(N+\nu)}$. Each channel use consists of an $N$ symbol burst transmission. The total average power radiated from all antennas and all time samples is constrained to less than $P_T$. Some definitions will be be helpful for clarity. We will compare the capacity behavior of several channel configurations. All SISO channel antennas comprise a subset of the antennas that participate in a SIMO (or MISO) channel, which in turn comprise a subset of the MIMO channel antennas. The capacity values for each of these channel configurations are denoted by $C_{1,1}$, $C_{M_R,1}$, $C_{1,M_T}$, and $C_{M_R,M_T}$, respectively. The singular value decomposition (SVD) of $\boldsymbol{H} = \boldsymbol{U}_H\boldsymbol{\Lambda}_H\boldsymbol{V}_H^*$, with the $n$th singular value denoted by $\lambda_{H,n}$. The spatio-temporal covariance matrix for $\boldsymbol{z}(k)$ is $\boldsymbol{R}_Z$ with eigenvalue decomposition $\boldsymbol{U}_Z\boldsymbol{\Lambda}_Z\boldsymbol{U}_Z^*$ and eigenvalues $\lambda_{Z,n}$.

*Theorem 1:* The information capacity for the discrete-time spatio-temporal communication channel $(\boldsymbol{H})$ is given by

$$C_{M_R,M_T} = \frac{1}{N}\sum_{n=1}^{K}\log\left(1+\frac{\lambda_{Z,n}|\lambda_{H,n}|^2}{\sigma^2}\right) \text{ bits/transmission} \tag{5}$$

where $\lambda_{Z,n}$ is found from the spatio-temporal water-filling solution[6]

$$\lambda_{Z,n} = \left(\xi - \frac{\sigma^2}{|\lambda_{H,n}|^2}\right)^+. \tag{6}$$

[4]SNR is defined here as the mean SNR per SISO channel dimension averaged over all matrix subchannels $\boldsymbol{H}_{i,j}$ within $\boldsymbol{H}$, i.e., $\text{SNR} \equiv (P_T/NM_TM_R\sigma^2); \Sigma_{i=1}^{M_R}\Sigma_{j=1}^{M_T}\Sigma_{n=1}^{N}|\lambda_{H_{i,j},n}|^2$.

[5]The results can easily be extended to the correlated spatio-temporal interference plus noise case with a prewhitening receiver filter matrix approach.

[6]The function $(\cdot)^+$ is equal to the argument if the argument is positive and is zero if the argument is negative.

*Proof:* Given the matrix description we have adopted for the spatio-temporal channel, the capacity proof is a simple extension of the well-known capacity result for SISO channels with memory [15]. ■

Theorem 1 suggests an extension of the temporal vector coding proposed by Kasturia *et al.* [16]. By choosing up to $K$ spatio-temporal transmission sequences $\boldsymbol{z}(k)$ that are multiples of the right singular vectors of $\boldsymbol{H}$, and receiving with up to $K$ matched spatio-temporal filter vectors that are the left singular vectors of $\boldsymbol{H}$, up to $K$ parallel subchannels are constructed.[7] We coin this structure STVC. The STVC parallel channel is written

$$\boldsymbol{\mathcal{X}}(k) = \boldsymbol{V}_H^* \boldsymbol{H} \boldsymbol{U}_H \boldsymbol{\mathcal{Z}}(k) + \boldsymbol{\mathcal{N}}(k) = \boldsymbol{\Lambda_H} \boldsymbol{\mathcal{Z}}(k) + \boldsymbol{\mathcal{N}}(k). \quad (7)$$

We now compare the asymptotic high SNR capacity behavior of the wireless channel for various antenna configurations. To simplify the discussion, we make the assumption[8] that $N \gg \nu$ so that the subchannel count bound (4) is well approximated by $K \approx N \cdot \min(L, M_T, M_R)$.

*Definition:* The *full rank assumption* is defined as the case where equality is achieved in the subchannel count bound.

*Corollary 1:* If multiple ports exist at only the input or only the output of the far-field spatio-temporal communication channel $(\boldsymbol{H})$, then as SNR increases, the capacity improvement as compared to that of any underlying SISO channel $(\boldsymbol{H}_{i,j})$ approaches a constant. For SIMO channels the constant is given by

$$C_{M_R,1} - C_{1,1} \to \frac{1}{N} \sum_{n=1}^{N} (\log |\lambda_{H,n}|^2 - \log |\lambda_{H_{i,j},n}|^2) \geq 0 \quad (8)$$

with a similar expression holding for MISO channels.

*Proof:* For the SIMO channel, define $\boldsymbol{H}_{i,1}$ as the $i$th SISO subchannel entry in $\boldsymbol{H}$. From Lemma 1, the rank$(\boldsymbol{H}) \leq N$. Thus, increasing the number of antennas at the output of the channel does not increase parallel channel opportunities for transmission. Choosing to transmit over $\boldsymbol{H}_{i,1}$ is a subset of the transmission solutions available given $\boldsymbol{H}$; therefore, $C_{M_R,1} - C_{1,1} \geq 0$. We define $\lambda_{\min}$ as the smallest singular value amplitude in either $\boldsymbol{H}_{i,1}$ or $\boldsymbol{H}$. The water-filling solution (6) uses all available subchannels when the transmit power exceeds

$$P_T > \frac{N\sigma^2}{|\lambda_{\min}|^2} - \sum_{n=1}^{N} \frac{\sigma^2}{|\lambda_{H,n}|^2}.$$

Defining $P_0 = N\sigma^2/|\lambda_{\min}|^2$, the asymptotic high SNR water-filling power distribution for both channels is

$$\lambda_{Z,n} \underset{P_T \gg P_0}{\longrightarrow} \frac{P_T}{N}.$$

[7] Note that the equivalent STVC receiver noise vector is still white due to the orthogonality of the right singular vector matrix $\boldsymbol{V}_H$.

[8] This assumption eliminates the mathematical inconvenience of dealing with the ratio $N+\nu/N$ that would otherwise appear in Corollary 1, Corollary 2, and the proofs when $M_T \geq \min(L, M_R)$.

Therefore, we can write

$$\begin{aligned} C_{M_R,1} - C_{1,1} &\underset{P_T \gg P_0}{\longrightarrow} \frac{1}{N} \sum_{n=1}^{N} \left[ \log\left(1 + \frac{P_T |\lambda_{H,n}|^2}{N\sigma^2}\right) \right. \\ &\qquad \left. - \log\left(1 + \frac{P_T |\lambda_{H_{i,1,n}}|^2}{N\sigma^2}\right) \right] \\ &\underset{P_T \gg P_0}{\to} \frac{1}{N} \sum_{n=1}^{N} [\log |\lambda_{H_n}|^2 \\ &\qquad - \log |\lambda_{H_{i,1,n}}|^2] \geq 0. \end{aligned}$$

Repeating the above argument for the MISO channel concludes the proof. ■

The capacity slope of a communication channel is now defined as the increase in capacity that results from multiplying the SNR by a constant factor $\eta > 1$

$$\Delta C_{M_R,M_T}(\eta) = C_{M_R,M_T}(\eta \,\mathrm{SNR}) - C_{M_R,M_T}(\mathrm{SNR}).$$

*Corollary 2:* If multiple ports exist at both the input and output of the spatio-temporal communication channel $(\boldsymbol{H})$, then as the SNR increases, the capacity slope for the MIMO channel approaches a constant $\rho \geq 1$ times the capacity slope for any underlying SISO, SIMO, or MISO channel. Under the full rank assumption, the asymptotic capacity slope multiplier is given by

$$\rho \to \min(L, M_R, M_T). \quad (9)$$

Thus, the capacity advantage of MIMO channel structures can grow without bound as SNR increases provided that multipath is present.

*Proof:* Following the first steps in the previous proof, we can easily show

$$\begin{aligned} C_{M_R,M_T} &\underset{P_T \gg P_0}{\longrightarrow} \frac{1}{N} \sum_{n=1}^{K} \log(|\lambda_{H,n}|^2) \\ &\qquad + \frac{K}{N} \log\left(\frac{1}{K\sigma^2}\right) + \frac{K}{N} \log(P_T) \end{aligned}$$

which leads directly to

$$\Delta C_{M_R,M_T}(\eta) \underset{P_T \gg P_0}{\longrightarrow} \frac{K}{N} \log(\eta).$$

In an identical manner, we find

$$\Delta C_{M_R,1}(\eta) \underset{P_T \gg P_0}{\longrightarrow} \log(\eta).$$

Repeating the above for MISO and SISO channels concludes the proof. ■

Corollaries 1 and 2 are somewhat surprising. Multipath is an advantage in far-field MIMO channels. If there is no multipath $(L = 1)$, then the high SNR capacity advantage of MIMO communication structures is limited to a constant improvement in bits as compared to SISO channels. If the multipath is severe $(L > \min(M_R, M_T))$, the high SNR capacity can essentially be multiplied by adding antennas to both sides of the radio link. This capacity improvement occurs with no penalty in average radiated power or frequency bandwidth because the number of parallel channel dimensions is increased. In contrast, adding

multiple antennas to only one side of the radio link increases capacity by an additive term as compared to SISO channels regardless of the number of propagation paths. This is because the number of parallel dimensions is not increased. This clearly provides theoretical motivation for optimal space–time communication structures that can be implemented in practice. In the next section we develop a practical computationally efficient approach to spatio-temporal coding that can achieve the multiplicative capacity advantage.

## IV. Discrete Matrix Multitone

The main disadvantage with the space–time vector coding solution is the associated computational complexity. The SVD of an $(N+\nu)M_R \times NM_T$ matrix must be computed. Complexity can be reduced by using a coding structure similar to the discrete multitone (DMT) solution for the SISO channel [17]–[19]. This new space–frequency coding structure results in a matrix of transmission and reception vector solutions for each discrete Fourier transform (DFT) frequency index. We therefore coin the method DMMT.

For DMMT, $N$ data symbols are again transmitted from each antenna during each channel usage. However, a cyclic prefix is added to the beginning of the data sequence so that the last $\nu$ data symbols are transmitted from each antenna element before transmitting the full block of $N$ symbols. By receiving only $N$ time samples at the output of each antenna element, ignoring the first and last $\nu$ output samples, the DMMT channel submatrices $\hat{\boldsymbol{H}}_{i,j} \in \mathbb{C}^{N\times N}$ now appear as cyclic structures. The new block cyclic channel matrix can again be written as the matrix sum in (2) with the Toeplitz pulse shaping matrices $\boldsymbol{G_l}$ replaced by the $N \times N$ cyclic pulse shaping matrices given in (10), shown at the bottom of the page. Given the cyclic SISO channel blocks, we can diagonalize the new channel matrix with a three-step procedure. We first post-multiply $\hat{\boldsymbol{H}}$ with the $NM_T \times NM_T$ block diagonal inverse discrete Fourier transform (IDFT) matrix

$$\boldsymbol{F}^{*(M_T)} = \begin{bmatrix} \boldsymbol{F}^* & & \\ 0 & \ddots & 0 \\ & & \boldsymbol{F}^* \end{bmatrix}$$

where each diagonal block is the unitary $N$ by $N$ IDFT matrix $\boldsymbol{F}^*$. The next step is to premultiply $\hat{\boldsymbol{H}}$ by a similar $NM_R$ by $NM_R$ block diagonal DFT matrix $\boldsymbol{F}^{(M_R)}$ where the diagonal submatrices $\boldsymbol{F}$ are $N$ by $N$ DFT matrices. With the well-known result [20] that the DFT basis vectors form the orthonormal singular vectors of the cyclic matrices $\hat{\boldsymbol{H}}_{i,j}$, the new matrix is

$$\boldsymbol{F}^{(M_F)}\hat{\boldsymbol{H}}\boldsymbol{F}^{*(M_T)} = \begin{bmatrix} \hat{\boldsymbol{\Gamma}}_{1,1} & \cdots & \hat{\boldsymbol{\Gamma}}_{1,M_T} \\ \vdots & \ddots & \vdots \\ \hat{\boldsymbol{\Gamma}}_{R_r,1} & \cdots & \hat{\boldsymbol{\Gamma}}_{M_R,M_T} \end{bmatrix}$$

where $\hat{\boldsymbol{\Gamma}}_{i,j}$ is the diagonal matrix containing the eigenvalues $\gamma_{i,j}(n)$ of the cyclic channel submatrix $\hat{\boldsymbol{H}}_{i,j}$. Premultiplication and post-multiplication by a permutation matrix $\boldsymbol{P}_R$, and post-multiplication by a similar permutation matrix $\boldsymbol{P}_T$, yields the block diagonal matrix

$$\boldsymbol{P}_R\boldsymbol{F}^{(M_R)}\hat{\boldsymbol{H}}\boldsymbol{F}^{*(M_T)}\boldsymbol{P}_T = \begin{bmatrix} \boldsymbol{\mathcal{H}}(1) & & \\ 0 & \ddots & 0 \\ & & \boldsymbol{\mathcal{H}}(N) \end{bmatrix} \tag{11}$$

where

$$\boldsymbol{\mathcal{H}}(n) = \begin{bmatrix} \hat{\gamma}_{1,1}(n) & \hat{\gamma}_{1,2}(n) & \cdots & \hat{\gamma}_{1,M_T}(n) \\ \hat{\gamma}_{2,1}(n) & \hat{\gamma}_{2,2}(n) & \cdots & \hat{\gamma}_{2,M_T}() \\ \vdots & \vdots & \vdots & \\ \hat{\gamma}_{M_R,1}(n) & \hat{\gamma}_{M_R,2}(n) & \cdots & \hat{\gamma}_{M_R,M_T}(n) \end{bmatrix}$$

is the $M_R \times M_T$ space–frequency channel evaluated at DFT index $n$.

It is instructive to explore the nature of the space–frequency channel matrix $\boldsymbol{\mathcal{H}}(n)$. Defining the receive array response vector as the column vector $\boldsymbol{a}_{R,l} = [a_{R,1}(\theta_{R,l}) \cdots a_{R,M_R}(\theta_{R,l})]^T$ and the transmit array response vector as $\boldsymbol{a}_{T,l} = [a_{T,1}(\theta_{T,l}) \cdots a_{T,M_T}(\theta_{T,l})]^T$, it can be verified that

$$\boldsymbol{\mathcal{H}}(n) = \sum_{l=1}^{L} \beta_l \mathcal{G}_l(n) \boldsymbol{a}_{R,l}\boldsymbol{a}_{T,l}^T \tag{12}$$

where $\mathcal{G}_l(n)$ is the DFT of the sequence $\{g_l(n)\}$ evaluated at DFT index $n$. Thus, at each frequency index, the DMMT channel is due to a weighted sum over $L$ rank-1 outer products of the frequency-invariant receive and transmit array response vectors. The weighting is determined by the frequency-invariant path fading values and the Fourier transform of the delayed pulse shaping function. This reveals a highly structured nature for the space–frequency channel spectrum.

Given the SVD of $\boldsymbol{\mathcal{H}}(n) = \boldsymbol{V}_{\mathcal{H}}(n)\boldsymbol{\Lambda}_{\mathcal{H}}(n)\boldsymbol{U}_{\mathcal{H}}^*(n)$, the diagonal DMMT channel matrix $\hat{\boldsymbol{H}}$ is finally obtained by

$$\hat{\boldsymbol{G}}_l = \begin{bmatrix} 0 & 0 & \cdots & 0 & g_l(\nu) & \cdots & g_l(2) & g_l(1) & g_l(0) \\ g_l(0) & 0 & 0 & \cdots & 0 & g_l(\nu) & \cdots & g_l(2) & g_l(1) \\ g_l(1) & g_l(0) & 0 & 0 & \cdots & 0 & g_l(\nu) & \cdots & g_l(2) \\ & \cdot & \cdot & \cdot & \cdot & & & & \\ & & \cdot & \cdot & \cdot & \cdot & & & \\ & & & \cdot & \cdot & \cdot & \cdot & & \\ & & & & \cdot & \cdot & \cdot & \cdot & \\ & & & & & \cdot & \cdot & \cdot & 0 \\ 0 & \cdots & 0 & g_l(\nu) & \cdots & g_l(2) & g_l(1) & g_l(0) & 0 \end{bmatrix}. \tag{10}$$

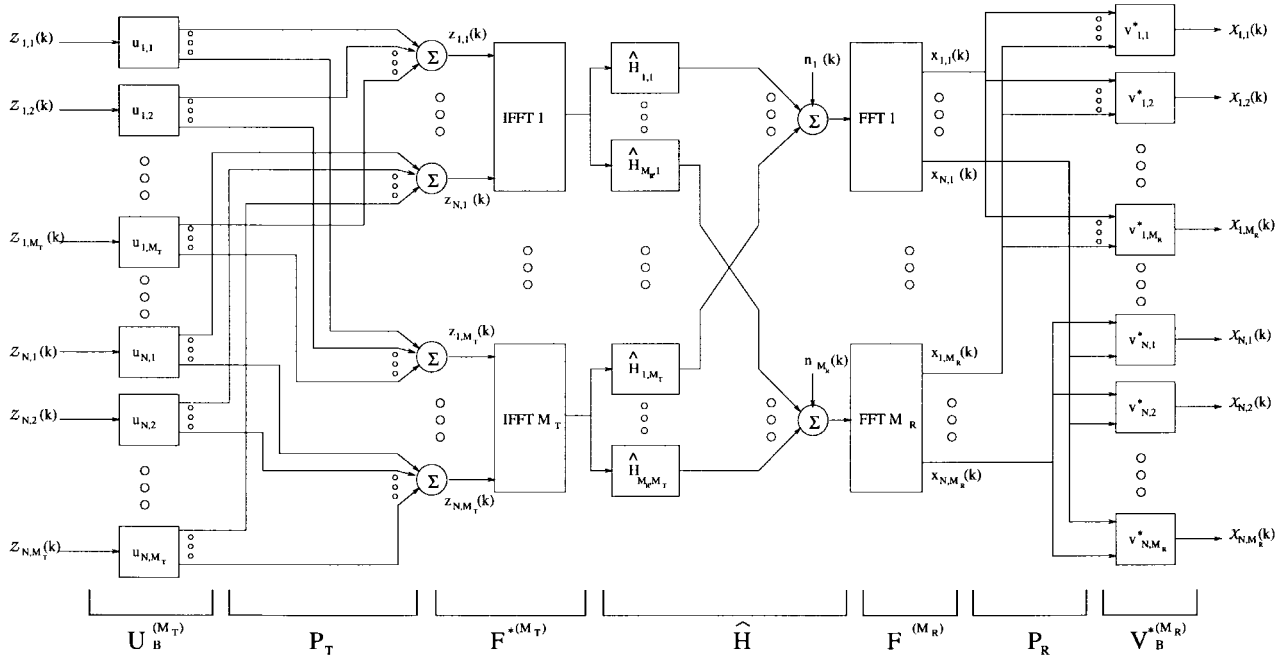


Fig. 4. DMMT system diagram.

postmultiplying by $\boldsymbol{U}_{\mathcal{H}}^{(M_T)}$ and premultiplying by $\boldsymbol{V}_{\mathcal{H}}^{*(M_R)}$

$$\begin{aligned}\boldsymbol{\Lambda}_{\hat{H}} &= \boldsymbol{V}_{\mathcal{H}}^{*(M_R)}\boldsymbol{P}_R\boldsymbol{F}^{(M_R)}\hat{\boldsymbol{H}}\boldsymbol{F}^{*(M_T)}\boldsymbol{P}_T\boldsymbol{U}_{\mathcal{H}}^{(M_T)} \\ &= \begin{bmatrix} \boldsymbol{\Lambda}_{\mathcal{H}}(1) & & \\ 0 & \ddots & 0 \\ & & \boldsymbol{\Lambda}_{\mathcal{H}}(N) \end{bmatrix}\end{aligned}$$

where $\boldsymbol{U}_{\mathcal{H}}^{(M_T)}$ is block diagonal, with each block containing the right singular matrices of the $\boldsymbol{\mathcal{H}}_n$ matrices, $\boldsymbol{V}_{\mathcal{H}}^{(M_R)}$ is block diagonal containing the left singular matrices of the $\boldsymbol{\mathcal{H}}_n$ matrices, and each of the diagonal submatrices $\boldsymbol{\Lambda}_{\hat{H}}$ contains the DMMT spatial subchannel amplitudes $\lambda_{\hat{H},i}$ where $\lambda_{\mathcal{H},j}(n) = \lambda_{\hat{H},(n\cdot M_R+j)}$. The parallel channel DMMT equation is then

$$\boldsymbol{\mathcal{X}}(k) = \boldsymbol{\Lambda}_{\mathcal{H}}\boldsymbol{\mathcal{Z}}(k) + \boldsymbol{\mathcal{N}}(k) \tag{13}$$

where $\boldsymbol{\mathcal{Z}}(k)$ is the length $M_TN$ input symbol vector, $\boldsymbol{\mathcal{X}}(k)$ is the length $M_RN$ output symbol vector, and $\boldsymbol{\mathcal{N}}(k)$ is the length $M_RN$ equivalent output noise vector. A block diagram architecture that implements the DMMT space–frequency channel decomposition is presented in Fig. 4.

Assuming $M_T = M_R = M$ and $N \gg \nu$, the $\mathcal{O}(N^3M^3)$ complexity of the vector coding solution computation has been reduced to $M$ independent $N$ point IFFT's, $M$ independent $N$ point FFT's, and $N$ independent $M$ by $M$ SVD's resulting in a complexity of $\mathcal{O}(MN\log N) + \mathcal{O}(NM^3)$ for DMMT. The signal processing complexity required at the transmitter and receiver to diagonalize all space–time subchannels for each data block has been reduced from $\mathcal{O}(N^2M^2)$ to $\mathcal{O}(MN\log N) + \mathcal{O}(NM^2)$.

We now show that STVC and DMMT are both asymptotically optimal.

*Theorem 2:* In the limit as $N \to \infty$, the capacity of the STVC solution and the DMMT solution both converge to the continuous-frequency channel capacity given by

$$C_0 = \int_{-\pi}^{\pi}\sum_{j=1}^{\rho}\log\left(1 + \frac{\lambda_{\mathcal{Z},j}(\omega)|\lambda_{\mathcal{H},j}(\omega)|^2}{\sigma^2}\right)d\omega \tag{14}$$

where $\lambda_{\mathcal{Z}_j}(\omega)$ is found from the space–frequency water-filling solution

$$\lambda_{\mathcal{Z},j}(\omega) = \left(\xi - \frac{1}{|\lambda_{\mathcal{H},j}(\omega)|^2}\right)^+. \tag{15}$$

*Proof:* The DMMT noise sequence is still AWGN since

$$\begin{aligned}\boldsymbol{R}_{\mathcal{N}} &= \boldsymbol{V}_{\mathcal{H}}^{*(M_R)}\boldsymbol{P}_R\boldsymbol{F}^{(M_R)} \\ &\quad\cdot(\sigma^2\boldsymbol{I})\boldsymbol{F}^{*(M_R)}\boldsymbol{P}_R^*\boldsymbol{V}_{\mathcal{H}}^{(M_R)} = \sigma^2\boldsymbol{I}_{N\cdot M_R}.\end{aligned}$$

Given this, and the parallel independent channel structure of DMMT, it is clear that

$$C_{DMMT} = \frac{1}{N}\sum_{n=1}^{N}\sum_{j=1}^{\rho}\log\left(1 + \frac{\lambda_{\mathcal{Z},j}(n)|\lambda_{\mathcal{H},j}(n)|^2}{\sigma^2}\right) \tag{16}$$

where

$$\lambda_{\mathcal{Z},j}(n) = \left(\xi - \frac{1}{|\lambda_{\mathcal{H},j}(n)|^2}\right)^+.$$

As $N \to \infty$, the noise sequence power spectrum remains flat with power density $\sigma^2$. It is well known that the DFT sequence converges to the continuous-frequency Fourier transform, so $\lim_{N\to\infty}\{\mathcal{G}_l(n)\} = \mathcal{G}_l(\omega)$,[9] which leads directly to

$$\boldsymbol{\mathcal{H}}(\omega) = \sum_{l=1}^{L}\beta_l\mathcal{G}_l(\omega)\boldsymbol{a}_{R,l}\boldsymbol{a}_{T,l}^T \tag{17}$$

[9]Note that $\mathcal{G}_l(\omega) = (1/T)\ \Sigma_{n=-\infty}^{\infty}\ [\mathcal{G}_{ct}((\omega/T)) - (2\pi n/T))e^{j(\omega/T-(2\pi n/T))\tau_l}]$ is the folded frequency spectrum of the continuous-time continuous-frequency Fourier transform $\mathcal{G}_{ct}(\omega) = \mathcal{F}(g(t-\tau_l))$.

and the channel matrix singular value $\lambda_{\mathcal{H},j}(n)$ becomes $\lambda_{\mathcal{H},j}(\omega)$. Therefore, from the standard properties of Riemann integration, the summation in (16) converges to the desired result for the DMMT structure.

For the STVC case, the output noise is again AWGN. With $\boldsymbol{H}$ written as in (2), it is known [21], [22] that the singular value distribution for the Toeplitz matrix $\boldsymbol{G}_l$ converges, as $N \to \infty$, to the continuous-frequency Fourier transform of $\{g_l(n)\}$. Therefore, the STVC space–frequency channel also converges to (17). This concludes the proof. ■

In the more general spatially continuous antenna case, the summation over the discrete antenna index $j$ becomes an integration over continuous antenna volume index $\psi$

$$\lambda_{\mathcal{Z}}(\omega,\psi) = \left(\xi - \frac{1}{|\lambda_{\mathcal{H}}(\omega,\psi)|^2}\right)^+ \tag{18}$$

$$C_0 = \int_{-\pi}^{\pi}\int_{\psi} \log\left(1 + \frac{\lambda_{\mathcal{Z}}(\omega,\psi)|\lambda_{\mathcal{H}}(\omega,\psi)|^2}{\sigma^2}\right) d\psi d\omega. \tag{19}$$

These equations suggest that an unexploited capacity multiplying advantage also exists for many distributed antenna structures commonly used in wireless communication.

## V. Spatio-Temporal Coding

This section provides background on existing coding schemes that can be used effectively to distribute information over parallel space and frequency (or temporal) dimensions that exist in STVC and DMMT channels. This discussion assumes estimation of the MIMO channel by transmitting a series of training symbol sequences from each antenna element and that the receiver and transmitter share the information required to decompose the channel into $K$ parallel subchannels. Estimating the DMMT channels can be accomplished by using well-known SISO channel training and estimation techniques for each of the channel subblocks $\boldsymbol{H}_{i,j}$.

The trellis codes first reported by Ungerboeck [23] led to the general class of coset coding techniques reported by Forney [24]. The coset selection encoder is typically a convolutional code with constraint length $\eta$ and input to output coding ratio $r$. The so-called "gap analysis" [25] provides an effective method for approximating the probability of error performance of coset codes. In this technique, a particular coset code with an associated lattice structure is characterized by first determining the SNR required to achieve a theoretical capacity equal to the desired data rate. The code gap is then the SNR multiplier required to achieve the target probability of error at the desired data rate. In a parallel channel communication system this gap can be used to determine the power and bit distributions that maximize data rate subject to a probability of error constraint. With a coding gap of $\alpha$, the rate maximizing water-filling solution for the DMMT channel becomes

$$\lambda_{\mathcal{Z}_{j,n}} = \left(\xi - \frac{\sigma_n^2\alpha}{|\lambda_{\mathcal{H},j}(n)|^2}\right)^+ \tag{20}$$

where $j$ is the spatial index and $n$ is the DFT frequency index. The bit allocation per subchannel is then given by

$$b_{j,n} = \log\left(1 + \frac{\lambda_{\mathcal{Z}_{j,n}}|\lambda_{\mathcal{H},j}(n)|^2}{\alpha\sigma_n^2}\right). \tag{21}$$

It is not possible to achieve infinite bit resolution (granularity) with coset codes. Therefore, the solution in (21) must be modified. Several bit loading algorithms exist to resolve this problem. The granularity of possible bit allocations is determined by the dimensionality of the coset code lattice structure. A two-dimensional symbol [e.g., quadrature amplitude modulation (QAM)] in an eight-dimensional lattice has a bit granularity of 0.25. In our MIMO channel communication structures the orthogonal constellation dimensions are the complex plane, space, and frequency (or time).

Referring now to [26], an effective coding method for parallel channel systems is to "code across subchannels." In this technique the power and bit allocation for each subchannel is computed as in (20) and (21), and each successive set of input bits to the trellis encoder corresponds to a different transmit subchannel. At each branch in the receiver's maximum-likelihood sequence estimator (MLSE) the number of possible coset members and trellis branches are determined by the number of bits loaded onto the corresponding subchannel. Using this technique, the maximum latency is approximately $5\eta + N + \nu$ [27]. The additive factor $N + \nu$ is associated with the decoding delay to code across transmitted data blocks. This factor can be eliminated using the so-called "tail biting" technique. If tail biting is used, there is a rate ratio penalty of approximately $N/N + 5\eta$ that is associated with always transmitting a known sequence at the end of the block so that the MLSE can complete the trellis decision sequence.

Many of the other practical coding techniques developed for parallel subchannel communication systems, not mentioned here, can also be applied to the STVC and DMMT parallel subchannel structures developed in the previous section.

## VI. Experimental Examples

In this section the results of wireless DMMT simulation experiments are reported. The first experiment compares the capacity of an example wireless MIMO channel with the capacity of the underlying SIMO and SISO channel blocks. The second experiment illustrates how DMMT can increase reliable data transmission rates using practical coding schemes. The third experiment illustrates the decrease in MIMO channel capacity that occurs if the number of multipath components is less than the number of input and output antenna elements.

*Example 1:*

The STVC channel is described by (2). For the DMMT channel, the block Toeplitz matrix $\boldsymbol{H}$ is replaced by the block cyclic matrix $\hat{\boldsymbol{H}}$. All model parameters are generated randomly from probability distributions that approximate a realistic urban multipath channel. There are ten random multipath components. The path time delays $\tau_l$ are drawn from a uniform distribution with a root-mean-square (rms) delay spread of 2 $\mu$s. The transmission and reception angles $\theta_{T,l}$ and $\theta_{R,l}$ for

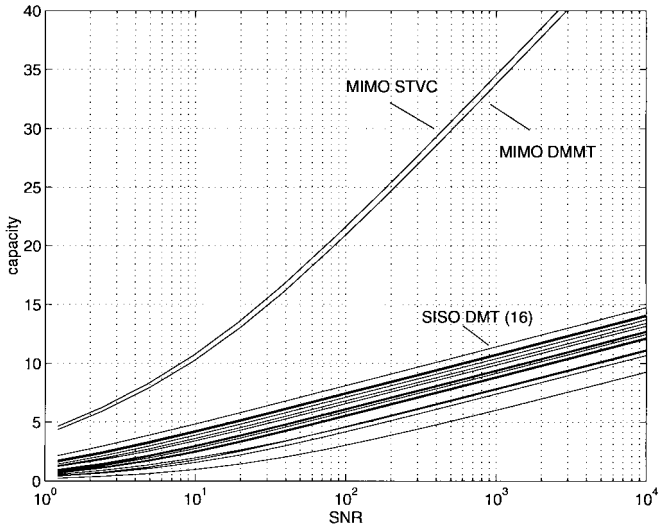


(a)

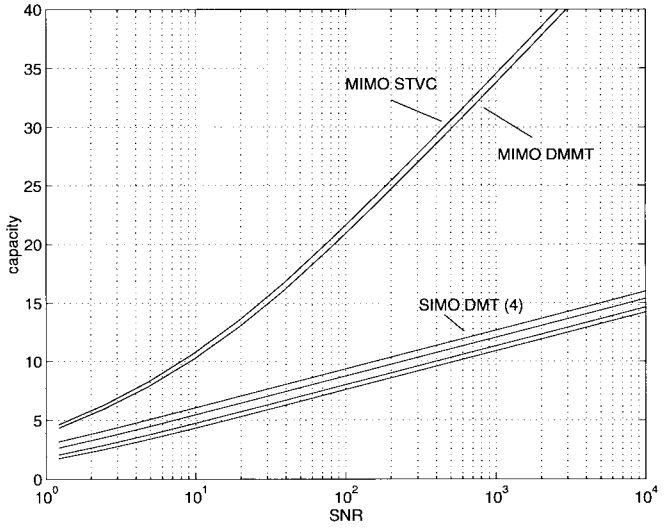


(b)

Fig. 5. Channel capacity experimental results for $L = 10$.

each path are drawn from uniform distributions centered at 0° with an rms angle spread of 25°. The path amplitudes $\beta_l$ are generated from a complex Gaussian distribution. The pulse shaping function $g(t)$ is raised cosine with 5-$\mu$s symbol period[10] and rolloff factor 0.35. The pulse function duration is seven symbol periods and the lag $\nu + 1 = 9$. Each antenna array contains four elements in a linear arrangement with an interelement spacing of five carrier frequency wavelengths. Each element has an omnidirectional radiation pattern. The number of transmitted symbols per block $N$ is 64. The receiver noise for each antenna element is complex AWGN.

The capacity of the 4×4 STVC channel is compared to the capacity of the 4×4 DMMT channel in Fig. 5. To provide a reference for capacity improvement, the capacity values for all 16 1×1 SISO DMT subchannels are computed. To provide another comparison, the capacity values for all 4×1 SIMO DMT channels are also computed. The transmitter power penalty associated with transmitting the cyclic prefix[11] is accounted for in the DMMT capacity results. Mean channel capacity per symbol[12] as a function of mean SNR[13] per symbol is plotted for each of the test cases.

The experimental results are in strong agreement with Corollaries 1 and 2. For large SNR values, a 3-dB increase in SNR results is a 4-bit increase in STVC channel capacity while the SISO [Fig. 5(a)] and SIMO [Fig. 5(b)] DMT channels only increase by 1 bit. This capacity slope multiplier corresponds to the fourfold increase in spatial channel water-filling dimensions associated with four channel inputs and four channel outputs. At all SNR values the DMMT channel capacity is significantly higher than the capacity of any of the SISO and SIMO DMT channels. The STVC channel capacity is slightly higher than the DMMT channel capacity. The difference is essentially equal to the transmitted power penalty associated with the cyclic prefix.

*Example 2:*

In the second example the same experimental channels described above are used again. The channels were evaluated for achievable data rates using the coding gap $(\alpha = 5$ dB) for a well-known eight-dimensional trellis code applied across space and frequency (time) subchannels. The results of the second experiment are presented in Table I. The experimental values for reliable data rate follow the same trends that were observed in the capacity experiments. The DMMT channel bit rate is much higher than all of the SIMO and SISO DMT channels. The high SNR DMMT data rate slope is again 4 bits per 3 dB SNR increase while the SIMO DMT and SISO DMT channels exhibit a slope of 1 bit per 3 dB increrase.

The experimental SISO multipath channels, with 300 kHz channel spacing, would support data rates ranging from 1.7 to 6.0 b/symbol period, or 0.34 to 1.20 Mb/s, at a mean SNR of 20 dB. This results in a data transmission efficiency from 1.1 to 4.0 b/s/Hz. When combined into a DMMT structure, these same underlying SISO channels with the same frequency bandwidth and transmitter power will support a data rate of 14.7 b/symbol period, or 2.94 Mb/s, for an efficiency of 9.8 b/s/Hz.

It may at first seem impractical to transmit an average of 15 b/symbol due to the limits of practical constellation sizes. However, the DMMT data for each DFT bin is spread over four orthogonal spatial subchannel dimensions. This reduces the peak number of bits per tone that must be transmitted over any single subchannel. With a mean SNR of 20 dB, the peak experimental data load for any single DMMT space–frequency subchannel is 7.2 b. The maximum data load for the best DMT SISO subchannel is 6.9 b and the maximum load for the best DMT SIMO subchannel is 8.1 b. Thus, even though

[10] This pulse shape is consistent with certain existing personal communication services (PCS) wireless modulation schemes intended for wireless local loop applications.

[11] The requirement to transmit the cyclic prefix results in an equivalent DMMT transmission power of $P_T \cdot N/(N + \nu)$.

[12] Mean capacity per symbol period is defined here as the total channel capacity in bits for all parallel channels over the entire block, divided by $N$.

[13] Mean SNR per symbol is computed by averaging over all of the squared channel singular values for all of the 16 SISO DMT channels and then multiplying by the ratio $P_T/\sigma_n^2$ (see footnote 4).

TABLE I
EXPERIMENTAL ACHIEVABLE DATA RATES AT $P_e = 10^{-6}$

| Experimental Case | R @ SNR=10 dB | R @ SNR=20 dB | R @ SNR=30 dB | R @ SNR=40 dB |
|---|---|---|---|---|
| Worst 1 by 1 SISO DMT | 0.4 bits/symbol | 1.7 bits/symbol | 4.1 bits/symbol | 7.0 bits/symbol |
| Best 1 by 1 SISO DMT | 3.0 bits/symbol | 6.0 bits/symbol | 9.0 bits/symbol | 12.1 bits/symbol |
| Worst 1 by 4 SIMO DMT | 2.6 bits/symbol | 5.5 bits/symbol | 8.6 bits/symbol | 11.6 bits/symbol |
| Best 1 by 4 SIMO DMT | 4.1 bits/symbol | 7.1 bits/symbol | 10.2 bits/symbol | 13.3 bits/symbol |
| 4 by 4 DMMT | 6.6 bits/symbol | 15.2 bits/symbol | 27.3 bits/symbol | 40.4 bits/symbol |
| 4 by 4 STVC | 7.0 bits/symbol | 15.8 bits/symbol | 28.0 bits/symbol | 41.1 bits/symbol |

the DMMT coding scheme achieves much higher data rates, in this experimental example, the maximum bit loading per tone was essentially the same as the best SISO channel and less than the best SIMO channel.

*Example 3:*

In the third example, a second capacity experiment was conducted wherein the number of multipath components was reduced to three, which is less than the four channel inputs and outputs. All other channel parameters remained unchanged from experiment 1. The results of this experiment are presented in Fig. 6. Again, the experimental data supports the theory on capacity slope. With only three multipath components, the maximum improvement in MIMO parallel space–time channel count is a factor of three above the SIMO and MISO channels. The high SNR DMMT capacity slope is now 3 bits for every 3 dB of SNR increase. The SISO and SIMO DMT channels maintain an incremental slope of 1 b per 3 dB SNR increase.

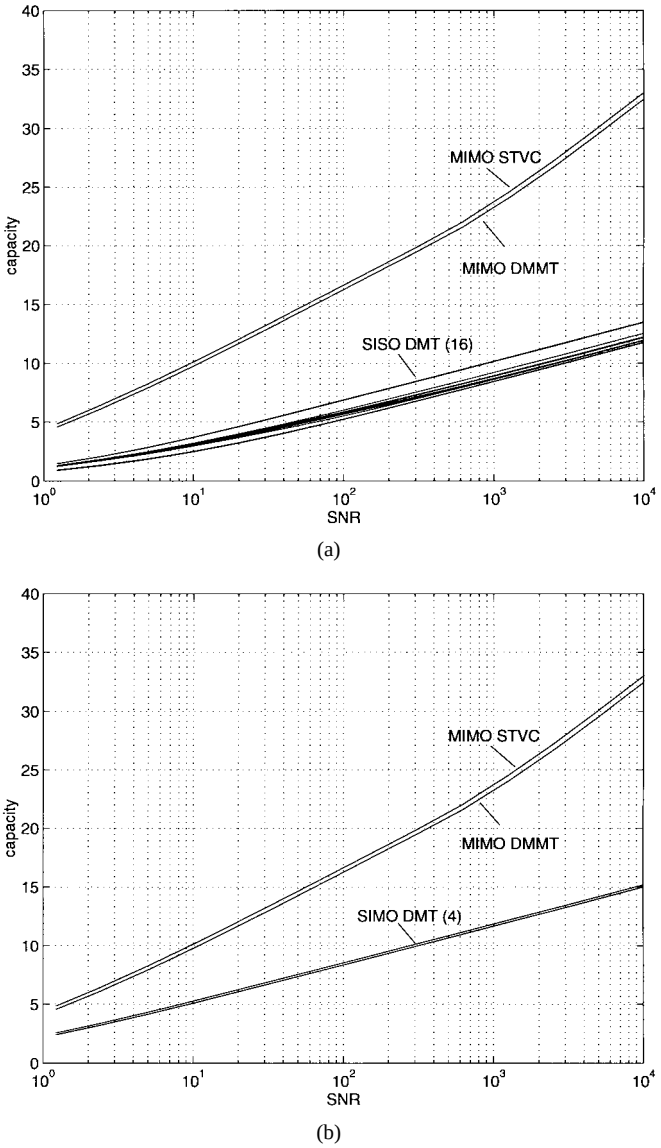


Fig. 6. Channel capacity experimental results for $L = 3$.

## VII. CONCLUSIONS

A model was developed wherein the difficult two dimensional problem of communicating with dispersive MIMO channels was collapsed into a one dimensional vector equation. The information capacity for wireless MIMO channels was then analyzed. An asymptotically optimal STVC communication structure was proposed. Multipath can significantly improve the capacity of MIMO channels. If $L > \min(M_R, M_T)$, then at high SNR values, the capacity slope in bits per decibel of power increase increases linearly with the number of antennas employed at the input and output of the channel. This capacity multiplying effect does not result from the well studied approach of employing multiple antennas only on one side of the channel. An asympototically optimal space–frequency MIMO DMMT information transmission structure was derived. This new approach has a complexity advantage of approximately $N^2$ as compared to STVC. The necessary background was provided to show how to use adaptive-lattice trellis-coding techniques to code across the space and frequency dimensions in a DMMT channel. Examples were provided to demonstrate that the theoretical results are consistent with observed experimental MIMO channel behavior.

The results presented in this paper can easily be extended to channels where the noise is not white but is highly structured as in the case of additive cochannel interference. In this case, large cellular network capacity gains result due to the ability to null interference at the receiver and the ability to constrain radiated interference power at the transmitter. Spatial coding techniques can also be applied to single frequency subchannel systems with flat fading, conventional analog multicarrier transmission channels, or CDMA channels where each code delay can be decomposed into orthogonal subchannels provided that there is subchip multipath. Our basic results can also be applied to a more general class of channels where the antenna array is distributed over large distances and the propagation does not follow far-field behavior. Finally, other

communication media such as wire-line, acoustic media, and optical media will experience the same basic communication system benefits when spatio-temporal MIMO channel structures are employed.

## ACKNOWLEDGMENT

The authors wish to thank Prof. D. C. Cox for discussions on mobile radio propagation theory. We would also like to thank T. Boros, R. Wesel, E. Ordentlich, and S. Diggavi for reviewing the manuscript.

## REFERENCES

[1] C. E. Shannon, "A mathematical theory of communications: Parts I and II," *Bell Syst. Tech. J.*, vol. 27, pp. 379–423, 623–656, 1948.
[2] L. H. Brandenburg and A. D. Wyner, "Capacity of the Gaussian channel with memory: The multivariate case," *Bell Syst. Tech. J.*, vol. 53, no. 5, pp. 745–78, May/June 1974.
[3] R. S. Cheng and S. Verdu, "Gaussian multiaccess channels with ISI: Capacity region and multiuser water-filling," *IEEE Trans. Inform. Theory*, vol. 39, pp. 773–785, May 1993.
[4] J. Salz, "Digital transmission over cross-coupled linear channels," *AT&T Tech. J.*, vol. 64, no. 6, pp. 1147–11159, July/Aug. 1985.
[5] A. Duel-Hallen, "Equalizers for multiple input multiple output channels and PAM systems with cyclostationary input sequences," *IEEE J. Select. Areas Commun.*, vol. 10, pp. 630–639, Apr. 1992.
[6] J. Yang and S. Roy, "On joint transmitter and receiver optimization for multiple-input-multiple-output (MIMO) transmission systems," *IEEE Trans. Commun.*, vol. 42, pp. 3221–3231, Dec. 1994.
[7] ———, "Joint transmitter-receiver optimization for multi-input multi-output systems with decision feedback," *IEEE Trans. Inform. Theory*, vol. 40, pp. 1334–1347, Sept. 1994.
[8] G. G. Raleigh, "Spatio-temporal coding in time varying wireless channels," Watkins-Johnson Co., Palo Alto, CA, Res. Rep., Jan. 1996.
[9] G. G. Raleigh and V. Jones, "Mulitvariate modulation and coding for wireless multimedia," submitted for publication.
[10] G. G. Raleigh, "MIMO multitone," Watkins-Johnson Co., Palo Alto, CA, Res. Rep., Feb. 1995.
[11] ———, "Discrete matrix multitone," Watkins-Johnson Co., Palo Alto, CA, Res. Rep., June 1995.
[12] G. G. Raleigh and J. M. Cioffi, "Spatio-temporal coding for wireless communications," in *Proc. 1996 Global Telecommunications Conference*, Nov. 1996, pp. 1809–1814.
[13] W. C. Jakes, *Microwave Mobile Communications*. New York: Wiley, 1974.
[14] D. C. Cox and R. P. Leck, "Distributions of multipath delay spread and average excess delay for 910 MHz urban mobile radio paths," *IEEE Trans. Antennas Propagat.*, vol. AP-23, pp. 206–213, Mar. 1975.
[15] T. M. Cover and J. A. Thomas, *Elements of Information Theory*. New York: Wiley, 1991.
[16] S. Kasturia, J. Aslanis, and J. M. Cioffi, "Vector coding for partial-response channels," *IEEE Trans. Inform. Theory*, vol. 36, pp. 741–62, July 1990.
[17] J. L. Holsinger, "Digital communication over fixed time-continuous channels with memory, with special application to telephone channels," *M.I.T. Res. Lab. Electron. Rep.*, vol. 430, p. 460, 1964.
[18] S. B. Weinstein and P. M. Ebert, "Data transmission by frequency-division multiplexing using the discrete fourier transform," *IEEE Trans. Commun.*, vol. COM-19, pp. 628–34, Oct. 1971.
[19] A. Ruiz, J. M. Cioffi, and S. Kasturia, "Discrete multiple tone modulation with coset coding for the spectrally shaped channel," *IEEE Trans. Commun.*, vol. 40, pp. 1012–29, June 1992.
[20] P. Lancaster, *Theory of Matrices*. New York: Academic, 1969.
[21] U. Grenander and G. Szego, *Toeplitz Forms and Their Applications*. Berkeley, CA: Univ. California Press, 1958.
[22] R. M. Gray, "On the asymptotic eigenvalue distribution of toeplitz matrices," *IEEE Trans. Inform. Theory*, vol. IT-18, pp. 725–730, June 1972.
[23] G. Ungerboeck, "Trellis-coded modulation with redundant signal sets: Parts I and II," *IEEE Commun. Mag.*, vol. 25, no. 2, p. 5–21, Feb. 1987.
[24] G. Forney, "Coset codes—Part I: Introduction and geometrical classification," *IEEE Trans. Inform. Theory*, vol. 34, pp. 1123–1151, Sept. 1988.
[25] G. D. Dudevoir, J. S. Chow, J. M. Cioffi, and S. Kasturia, "Vector coding for T1 transmission in the ISDN digital subscriber loop," in *IEEE Int. Conf. Communications*, Boston, MA, 1989, pp. 536–540.
[26] J. C. Tu, "Theory, design and application of multi-channel modulation for digital communications," Ph.D. dissertation, Stanford Univ., Stanford, CA, 1991.
[27] G. Forney, "Maximum-likelihood sequence estimation of digital sequences in the presence of intersymbol interference," *IEEE Trans. Inform. Theory*, vol. IT-18, pp. 363–378, May 1972.

**Gregory G. Raleigh** (M'87) received the B.S.E.E. degree from California Polytechnic State University, San Luis Obispo, CA, in 1984, and the M.S.E.E. degree in electrical engineering from Stanford University, Stanford, CA, in 1994. He is currently working toward the Ph.D. degree in electrical engineering from Stanford University, Stanford, CA.

He is Chief Technical Officer and a Cofounder of Clarity Wireless, Inc., Belmont, CA, where he oversees research and development for a new generation of broad-band wireless access modems that employ adaptive digital modulation and coding to enhance performance in severe multipath environments. Before joining Clarity, he was a Staff Scientist at Watkins Johnson Company, responsible for leading research, design, and development for a number of comercially successful microwave radio and radar products. He has several publications in the areas of advanced microwave radio techniques and adaptive multivariate signal processing for wireless communications. He also has several patents and pending patents in wireless communications.

**John M. Cioffi** (S'77–M'78–SM'90–F-96) received the B.S.E.E. degree from the University of Illinois, Urbana-Champaign, in 1978, and the Ph.D.E.E. degree from Stanford University, Stanford, CA, in 1984.

From 1978 to 1984 he was a Modem Designer with Bell Laboratories, and from 1984 to 1986 he was a Disk Read-Channel Researcher with IBM Corporation. Since 1986 he has been on the faculty of Stanford University, Stanford, CA, where he is currently a tenured Associate Professor. In 1991 he founded Amati Communications Corporation, San Jose, CA, where he has served as an Officer and Director, and where he is currently Chief Technical Officer in addition to his position at Stanford. His specific interests are in the area of high-performance digital transmission and storage systems. He has over 100 publications in this area and he holds 20 patents, all of which are licensed.

Dr. Cioffi received the 1991 *IEEE Communications Magazine* Best Paper Award and the 1995 T1 Outstanding Achievement Award of the American National Standards Institute. He was an NSF Presidential Investigator from 1987 to 1992. He has served in a number of editorial positions for IEEE magazines and conferences.